Disordered Exciton Analysis of Linear and Nonlinear Absorption Spectra of Antenna Bacteriochlorophyll Aggregates: LH2–Only Mutant Chromatophores of Rhodobacter sphaeroides at 8 K u...

ARTICLE *in* THE JOURNAL OF PHYSICAL CHEMISTRY B · OCTOBER 1999

Impact Factor: 3.3 · DOI: 10.1021/jp991676n

4 AUTHORS:

Arvi Freiberg
University of Tartu
132 PUBLICATIONS **2,336** CITATIONS
SEE PROFILE

Kõu Timpmann
University of Tartu
57 PUBLICATIONS **1,169** CITATIONS
SEE PROFILE

Rein Ruus
University of Tartu
33 PUBLICATIONS **353** CITATIONS
SEE PROFILE

Neal W Woodbury
Arizona State University
138 PUBLICATIONS **4,051** CITATIONS
SEE PROFILE

Disordered Exciton Analysis of Linear and Nonlinear Absorption Spectra of Antenna Bacteriochlorophyll Aggregates: LH2−Only Mutant Chromatophores of *Rhodobacter sphaeroides* at 8 K under Spectrally Selective Excitation

Arvi Freiberg,*,†,‡ Kõu Timpmann,†,‡ Rein Ruus,‡ and Neal W. Woodbury†

Department of Chemistry and Biochemistry and Center for the Study of Early Events in Photosynthesis, Arizona State University, Tempe, Arizona 85287, and Institute of Physics, University of Tartu, EE51014 Tartu, Estonia

Received: May 24, 1999

The objective of this work is two-fold. First, the effects of static diagonal disorder on the linear and nonlinear absorption spectra of excitons in circular molecular aggregates are studied by computer modeling. Second, it is demonstrated that this simplified model successfully reproduces the main features of both the ground-state absorption and initial pump−probe absorption difference spectra of LH2 antenna proteins from photosynthetic bacteria measured upon spectrally selective population of excitons at low temperature. Of the usual first-order approximations in the Frenkel exciton theory, our model exploits only two: the two-state and the zero electron−vibrational coupling approximations. In our model, the molecules of the aggregate are allowed to have different site energies. The coupling between all aggregate molecules is taken into account. An important difference between our study and previous work is that the exciton state selective spectra are calculated corresponding to the recently performed spectrally selective ultrashort pulse excitation experiment. We investigate the behavior of excitons as a function of disorder separately in the B850 and B800 ring aggregates of LH2. Usually, excitations in the B800 ring have been considered completely localized. The present study reinforces the importance of static diagonal disorder in describing the spectral properties of excitons in the LH2 antenna complex at low temperatures. Moreover, it has been demonstrated that two types of spectral disorder govern the inhomogeneously broadened exciton spectra of antenna complexes embedded into the photosynthetic membrane rather than a single source of disorder. From the comparison of simulated and experimental linear absorption spectra, we suggest that the peculiar asymmetry of the B800 band as well as some of the high-energy sideband structures are due to weak coupling of excitons in the B850 and B800 ring aggregates with intramolecular vibrations of bacteriochlorophyll *a* molecules.

1. Introduction

The main purpose of this work is to provide a better understanding of the optical spectroscopy of photosynthetic light-harvesting pigment−protein complexes, particularly bacteriochlorophyll−protein antennas. A deeper knowledge of spectroscopy allows one to draw more detailed conclusions about the nature of light excitations in the antennas and about the intermolecular couplings governing their dynamics.

In photosynthetic membranes, antenna complexes serve to carry out very efficient solar energy absorption and transfer into the photochemical reaction center where the transduction to chemical energy occurs. The exact nature of the antenna excitations has been studied for many years but remains a matter of considerable debate. Due to a high density of chlorophyll molecules and the resulting strong coupling between them, it seems natural that the excitations take the form of excitons, delocalized over many antenna molecules. However, the experimental evidence has been limited as yet. One reason for this is the well-documented inhomogeneous broadening of in vivo chlorophyll spectra due to spectral disorder.[1−3] Inhomogeneous broadening essentially obscures the detailed exciton effects.

Current high-resolution X-ray crystal structures of the peripheral antenna pigment−protein complex (LH2) from photosynthetic purple bacteria allow a more sophisticated analysis of this problem. The basic unit of the LH2 antenna complex is a pair of membrane spanning helical α and β polypeptides. In *Rhodopseudomonas (Rps.) acidophila*, nine $\alpha\beta$-polypeptide pairs form a cylindrical arrangement that accommodates two rings of bacteriochlorophyll *a* (BChl) molecules,[4] B800 and B850, labeled according to their long-wavelength Q_y absorption peaks at about 800 and 850 nm, respectively. The B850 ring constitutes the main port for energy transfer from the peripheral LH2 antenna to the core (LH1) antenna surrounding the reaction center. The B850 ring includes 18 closely spaced BChl molecules in a waterwheel like arrangement. The Q_y-transition dipoles of the B850 BChls are orientated nearly on the ring plane, while the porphyrin planes of the molecules are perpendicular to the plane of the membrane. The Mg−Mg distance between the adjacent BChl molecules alternates repeatedly between 0.89 and 0.96 nm (the closest approach between the BChls being about 0.4 nm). The B800 ring is an array of 9 BChls with 2.12 nm separation between the adjacent molecules. The BChls in the B800 and B850 rings are relatively well

* Address correspondence author at the Institute of Physics, University of Tartu, EE51014 Tartu, Estonia. E-mail: freiberg@fi.tartu.ee. Phone: +372-7-383024. Fax: +372-7-383033.

† Arizona State University.

‡ University of Tartu.

10.1021/jp991676n CCC: $18.00
Published on Web 10/26/1999

isolated from each other. The closest Mg−Mg separation between the BChls in different rings is 1.76 nm. A comprehensive review of the relationship between the LH2 complex structure and elementary excitation dynamics has just appeared.[5]

Delocalized excitons are the elementary optical excitations of nanoaggregates of coupled molecules.[6,7] It is frequently assumed that the constituent molecules of the aggregate are characterized by a single electronic transition only. This so-called two-level approximation applies when the transition under consideration is energetically well separated from the rest of the transitions. As a further simplification, the exciton−phonon coupling is usually neglected. With these assumptions, the excitonic Hamiltonian for N coupled molecules can be written as[6,7,8−12]

$$\hat{H} = \sum_{i}^{N} \hat{H}_i + \sum_{i<j}^{N} V_{ij} \tag{1}$$

where $\hat{H}_i$ is the electronic Hamiltonian for molecule i and V_{ij} represents the resonant coupling between molecules i and j. The diagonal elements of the matrix $\hat{H}$ give the energies of uncoupled molecules or the site energies, which can be represented as

$$H_{ii} = E + D + \delta_i \tag{2}$$

Here E is the electronic transition energy of the free molecule, D is the solvent shift caused by the interactions of the molecule with its environment, and δ_i is the random offset energy due to the static and dynamic fluctuations of the environment. D is the origin of large-scale spectral heterogeneities, while δ_i is responsible for a gentler inhomogeneous broadening of the spectra. The off-diagonal elements of the matrix $\hat{H}$ give the intersite coupling energies that cause the single-site excitations to spread over all molecules of the aggregate. The characteristics of exciton motion depend on the relative magnitude of the coupling energy and perturbing disorder. In this work, we neglect the off-diagonal disorder, because it is expected to cause a Lorentzian-like low-energy tail of the absorption spectrum,[8] which has not been observed in LH2. It has been shown[8] that in linear aggregates the total disorder-induced band shift is the sum of the shifts caused by the diagonal and off-diagonal disorder separately, whereas the absorption bandwidth is the geometrical mean of the separate bandwidths. This prescription corresponds to the addition of independent Gaussian disorder distributions. Methods of calculating the aggregate spectra based on the Hamiltonian matrix (1) are well developed,[8−13] and their reliability is successfully tested in the case of linear aggregates, notably the J-aggregates.[8,14] Despite the great activity,[15−23] understanding of the optical properties of the disordered photosynthetic chromophore aggregates, including LH2 complexes, has been more limited. This is the prime motivation of the present work.

Recently, we have been studying the LH2 complexes from the purple non-sulfur photosynthetic bacterium *Rhodobacter (Rb.) sphaeroides* by using a novel approach.[24,25] First, a transient pump−probe absorption technique, characterized by simultaneous femtosecond temporal and nearly transform-limited spectral resolution (femtosecond spectrochronography), was applied. Second, excitons were selectively excited in the B850 aggregate of BChl molecules by pulses of 4−5 nm spectral bandwidth tuned over the whole B850 ground-state absorption spectrum between 820 and 880 nm. The transient transmission spectra were measured over a 140 nm spectral range using a white light continuum probe pulse. Third, measurements were performed at low temperatures down to 8 K. A strong effect of dynamic spectral hole burning was observed, the shape of the transient spectrum being strongly excitation wavelength-dependent. Only a very narrow initial bleaching contour was observed when pumped in the region of 840−850 nm. Spectra excited to the blue of this wavelength region revealed a more complex structure. The time evolution of the transient spectra in the femtosecond and picosecond time range depended on both the pump and probe wavelengths. The following conclusions have been drawn from these studies: (i) The dependence of the initial (time zero) spectra on pump wavelength is mostly due to exciton-state selection within the ensemble of disordered excitons. (ii) The early spectral dynamics is a result of an inter-exciton state relaxation plus the exciton transfer between different LH2 complexes.

Below, we shall analyze the linear and nonlinear absorption spectra of excitons in the LH2 antenna of *Rb. sphaeroides* using computer simulations. An important difference between our study and previous work is that the exciton state selective spectra are calculated, corresponding to the spectrally selective ultrashort pulse excitation experiment.[24,25] We investigate the behavior of excitons as a function of disorder, both in the B850 and B800 rings of LH2. Usually, excitations in the B800 ring have been considered completely localized. At low temperatures at least, this viewpoint is not warranted. The standard approximation of neglecting exciton−phonon coupling seems to be appropriate in the B850 ring where at low temperatures the exciton coupling energy and splitting between the exciton levels is large compared to both the dephasing-induced width of the levels and to the exciton−phonon coupling energy.[26] We shall see that the situation is much less clear in the case of the B800 ring where the exciton coupling energy is an order of magnitude less than in the B850 ring.[3] Considering the nonlinear absorption spectra, the present work is limited to modeling of the initial exciton state only and, thus, to reproduce the initial exciton spectra. A relaxed exciton state, which is important for the simulation of the exciton fluorescence emission spectrum and the passage between the prompt and relaxed states (the dynamics of the system), will be discussed in our forthcoming paper.

2. Model Assumptions and Computational Algorithms

The structure of the antenna proteins from *Rb. sphaeroides* is not known as yet. Therefore, we have made use of the established coordinates and orientations of the transition dipole moment unit vectors in the LH2 complex from *Rps. acidophila*.[4] Each BChl molecule is modeled by a single Q_y optical transition. Dense packing of BChls in the LH2 structure implies that not only nearest neighbors but also other molecules in the ring may be effectively coupled to each other. For generality, in the following simulations, the explicit mechanism of the couplings is left open. However, a simplifying assumption was made that different pairwise coupling energies between the BChl molecules relate according to the familiar dipole−dipole interaction formula

$$V_{ij} = 5.04\mu^2\kappa_{ij}/\epsilon R_{ij}^{\ 3} \tag{3}$$

where the orientation factor κ_{ij} is defined as

$$\kappa_{ij} = \vec{\mu}_i \cdot \vec{\mu}_j - 3(\vec{\mu}_i \cdot \vec{R}_{ij})(\vec{\mu}_j \cdot \vec{R}_{ij}) \tag{4}$$

In eqs 3 and 4, μ^2 gives the dipole strength of the isolated molecule, $\vec{\mu}_j$ is the unit vector associated with the transition moment of the jth molecule in the aggregate, ϵ is the dielectric constant of the medium (relative permittivity), $\vec{R}_{ij}$ is the unit

vector along the line joining the two transition dipoles, and R_{ij} is the distance between the two dipoles. If the distance and transition dipole moments are measured, respectively, in nanometers and debye units, the coupling in eq 3 is read in wavenumbers.

The linear (ordinary ground state) absorption spectrum of the aggregate is calculated as a sum of individual transitions from the ground state $|0\rangle$, where no molecule is excited, to the one-exciton states $|k\rangle$

$$A(E) = \sum_{k}^{N} A_k(E) \tag{5}$$

Individual transitions in eq 5 are characterized by homogeneous line shapes $A_k(E)$ and subject to the normalization condition $\int A_k(E)\, \mathrm{d}E = A_k$. The dipole strengths A_k can be calculated as $A_k = \mu^2|c_1^k\vec{\mu}_1 + c_2^k\vec{\mu}_2 + ... + c_N^k\vec{\mu}_N|^2$ where the eigenvector expansion coefficients c_i^k specify the contribution of the ith excited site into the kth one-exciton state.[6,7]

The initial (that is, before significant energy relaxation and transfer have occurred) nonlinear pump−probe absorption difference spectrum is approximated with

$$\Delta A(E) = \sum_{k} \Delta A(E, k) \tag{6}$$

where the contribution of the one-exciton state $|k\rangle$ into the total spectrum is defined as

$$\Delta A(E, k) = -A_k(E) - \sum_{m}^{N} A_m(E) + \sum_{l}^{N(N-1)/2} A_{k,ll}(E) \tag{7}$$

In eq 7, the first right-hand side term is the stimulated emission (SE) spectrum from the populated one-exciton state $|k\rangle$. The second expression gives the excitation-induced bleaching of the ground-state absorption spectrum (GSB). Finally, the third term represents the absorption spectrum from the excited state (ESA); i.e., it is caused by the transitions from the one-exciton state $|k\rangle$ to all possible two-exciton states $|ll\rangle$. The dipole strengths $A_{k,ll}$ can be evaluated as $A_{k,ll} = \mu^2|\sum_{i<j}^{N} \mathrm{d}_{ij}^l\, (c_i^k\vec{\mu}_j + c_j^k\vec{\mu}_i)|^2$. The normalization condition for $A_{k,ll}$ reads as $\int A_{k,ll}(E)\, \mathrm{d}E = A_{k,ll}$. The coefficients d_{ij}^l are obtained from the matrix of eigenvectors resulting from the diagonalization of the $N(N-1)/2$ times $N(N-1)/2$ two-exciton Hamiltonian matrix. The real and symmetric two-exciton matrix is completely described by the parameters of the one-exciton states.[11−14,20−22]

The SE and GSB contribute the negative (bleaching) part of the $\Delta A(E)$ spectrum, while the ESA donates the positive part. It is important to notice that the spectral shape of GSB in eq 7 is independent of the excitation pulse wavelength, whereas the SE and ESA spectra depend on the specific populated one-exciton states. Under short pulse excitation, SE and ESA transitions initiate only from the resonantly excited one-exciton levels. Relaxation between the one-exciton levels during the exciton lifetime (which is accounted for indirectly by the present model via the finite homogeneous width of the spectral lines, see below) transforms the SE and ESA spectra, but leaves the GSB spectrum unchanged.

The calculations begin with the numerical diagonalization of the one-exciton Hamiltonian in order to solve for the one-exciton transition energies and eigenvectors. The diagonal matrix elements of this Hamiltonian are the transition energies of the sites, whereas the resonant coupling energies of eq 3 serve as off-diagonal elements of the matrix. Adding random offset energies to the site energies according to eq 2 includes disorder. A particular array of transition energy offsets is obtained by means of a generator producing random numbers according to a normal distribution with predetermined mean and standard deviation. Once the eigenvectors have been calculated, the dipole strength of an individual transition is obtained. The distribution of dipole strengths of all one-exciton transitions gives the stick spectrum corresponding to the linear absorption. In order to explore the entire distribution of possible heterogeneous ring systems, the above procedure is repeated up to 5000 times for different sets of randomly chosen offset energies. The SE stick spectrum can be taken identical to the stick spectrum of the linear absorption, since the Einstein coefficients for stimulated emission and absorption are equal and the electron−phonon coupling is ignored. The basic procedure to find the ESA stick spectrum is similar. The major difference is that now a two-exciton Hamiltonian matrix should be diagonalized. Again, a normal distribution random number generator is used to set the diagonal offset energies. In this procedure, we explicitly assume that the ground state to one-exciton state transitions are totally uncorrelated with the one-exciton to two-exciton transitions.

The stick spectra of disordered rings are further dressed one by one with the homogeneous line shapes. We consider that the major cause of the homogeneous broadening of the exciton transitions is energy relaxation between the exciton states. Indeed, it has been shown[26,27] that in LH2, the pure dephasing-induced broadening has a minor role at the actual low temperatures. For simplicity, a uniform width of all lines has been assumed, except of the lines corresponding to the lowest-energy transition in every ring. The latter transition is expected to represent a sharper line, as the lowest state is the last rung of the interexciton state relaxation ladder. The width of the lines corresponding to the one-exciton to two-exciton transitions could be varied. In most cases, however, it has been taken the same or up to 2 times broader than the width of the high-energy one-exciton transition lines. As a rule, the Lorentzian homogeneous line shapes have been assumed.

Finally, the prompt $\Delta A(E)$ spectra allowing direct comparison with the experimental spectra are calculated. The initial population of the one-exciton states in resonance with the Gaussian excitation pulse is considered as the spectral overlap integral between the excitation pulse and the corresponding one-exciton absorption lines. These overlap integrals are proportional to the initial populations of the exciton states and allow for the prompt SE and ESA spectra to be calculated from these states. This procedure is repeated one by one for all disordered aggregates.

In this work, we consider the excitons in the B850 and B800 rings as well isolated, so that the B850 and B800 spectra are additive and can be calculated separately from each other. This seems to be justified by the experimental results[24,25] showing no bleaching of the B800 absorption band in *Rb. sphaeroides* when exciting in the B850 band. More extensive calculations including dipolar couplings between all the BChls in the LH2 structure await to be done. The computer programs for performing the calculations described above were written using Mathcad 7 (MathSoft) and FORTRAN language softwares.

3. Simulations

Our main interest in the present work is concentrated toward excitons in the B850 ring. Therefore, the demonstrations given below concern exclusively exciton spectra of the B850 aggregate. The results are presented in a relative energy scale, with the unit being the largest nearest-neighbor coupling energy. It is intended that the specific coupling energies can be found out by comparison with the experiment.

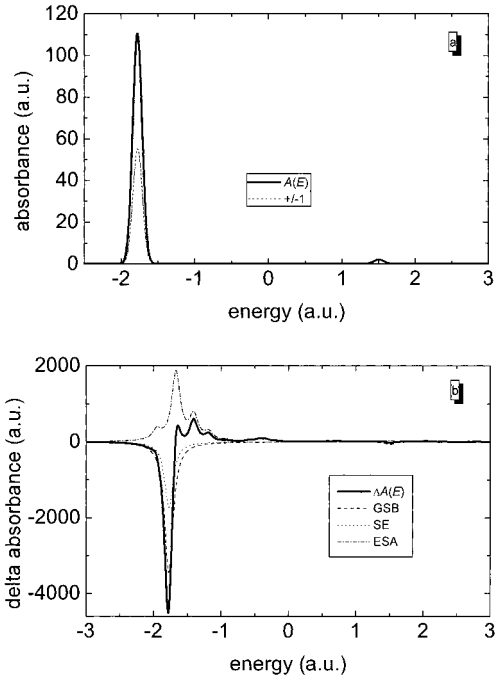

Figure 1. Simulated linear ground-state absorption spectrum $A(E)$ (a) and prompt nonlinear absorption difference spectrum $\Delta A(E)$ (b) together with the component spectra of a single ring of 18 transition dipoles mimicking a B850 aggregate. Individual transitions are characterized with the homogeneous fwhm: $\gamma_0 = 0.02$ and $\gamma = 0.15$. In part (a) only most prominent and degenerate $k = \pm 1$ component spectra are shown. See text for further details.

Single Ring of Transition Dipoles Mimicking Ideal B850 Without Disorder. The simplest B850 model that has relevance to our problem is a ring of 18 transition dipoles, spatially arranged similar to the BChl molecules in the B850 ring of LH2 in *Rps. acidophila* and all having the same transition energy. Figure 1a shows the ground-state exciton absorption spectrum, *A(E)*, of such ring together with the strongest composite spectra, $A_k(E)$, according to eq 5. The transition energies of isolated sites are arbitrarily taken to be zero. Gaussian homogeneous line shapes of the individual transitions having the same widths (full width at half-maximum (fwhm), $\gamma = 0.15$) have been assumed, including the one-exciton to two-exciton transitions accounted for in Figure 1b. The only exception, as was pointed out above, is the lowest-energy one-exciton transition with $\gamma_0 = 0.02$. The interaction matrix and the coordinates of the transition dipole moment unit vectors used were those of ref 21.

The one-exciton band in Figure 1a consists of two groups of 9 transitions arranged asymmetrically relative to the zero site energy. These Davydov (after Davydov[6]) manifolds appear because, according to our assumption, the 18 BChl molecules in the B850 ring are grouped by heterodimers as in *Rps. acidophila* with different coupling energies within and between the elementary dimers. According to the calculations performed by the authors of ref 21, the nearest-neighbor resonant coupling energies within the elementary dimer, V_i, and between the dimers, V_e, relate as $V_i/V_e \approx 1/0.68$. The asymmetry of the manifolds results from the non-nearest-neighbor couplings present in the system. The largest of the latter terms holds about 13% of V_i.[21] As a result of the geometrical constraint that the dipole moments of the two BChls in the $\alpha\beta$ heterodimer are almost exactly antiparallel, the lower manifold carries almost all absorption intensity. Furthermore, as all the transition dipoles are orientated almost on the ring surface, most of the oscillator strength is concentrated into the two next lowest $k = \pm 1$ degenerate transitions.[23] According to the present calculations, the transition to the lowest nondegenerate $k = 0$ exciton state carries only 3.6×10^{-5} of the total oscillator strength of the one-exciton absorption band. The latter is, of course, equal to 18 times the oscillator strength of an isolated BChl molecule. In contrast, the highest energy nondegenerate $k = 0$ transition is the strongest in the upper Davydov manifold. The linear-scale Figure 1a exposes only two overlapping $k = \pm 1$ transitions shaping the low-energy absorption band edge at -1.78 and a single $k = 0$ transition contributing primarily at $+1.5$, the high-energy edge of the absorption spectrum.

Figure 1b illustrates the prompt nonlinear absorption difference spectrum of the B850 ring, calculated according to eq 6. Excitation is into the maximum of the linear absorption spectrum at energy -1.78 using a Gaussian pulse with a width of $\Gamma_{ex} = 0.2$. This time, the exciton transitions have been assigned a more realistic Lorentzian shape with the same γ and γ_0 values as previously. Notice the characteristic shape of the $\Delta A(E)$ spectrum with the negative signal prevailing at the low-energy side and the positive one governing the opposite side of the spectrum. This is due to the spectral overlap of the ESA and GSB/SE spectra. As expected, the ESA spectrum is broader compared to the GSB spectrum. It also reveals a clear structure.

A Single Representative of the B850 Rings with Diagonal Disorder. Effects of diagonal disorder on the $A(E)$ and $\Delta A(E)$ spectra of a particular B850 ring picked up from an ensemble of disordered aggregates are demonstrated in Figure 2. The ensemble was generated assuming that the distribution function of the offset energies, $P(\delta_i) = P(0)\exp(-\delta_i^2/2\sigma^2)$, is characterized by a standard deviation of $\sigma = 0.72$. Other parameters applied to create Figure 2 are identical to the previous example.

As can be seen in Figure 2a, the disorder radically changes the intensity distribution of the linear absorption spectrum. Virtually all exciton transitions gain strength at the expense of the low-energy $k = \pm 1$ transitions, which dominate the spectrum of ideal B850 rings. Most notable is the considerable intensity attained by the lowest $k = 0$ transition (about 13%, if averaged over large ensemble, see below). Disorder also lifts the degeneracy of the doubly degenerate states, shifts the maximum of the spectrum toward lower energy, and fills in the gap between the Davydov manifolds. Finally, it leads to substantial (over 20%) broadening of the one-exciton band and, thus, the linear absorption spectrum.

Figure 2, b and c, shows two prompt $\Delta A(E)$ spectra of the disordered ring illustrating the effect of excitation wavelength on the absorption difference spectrum. Excitation demonstrated is at -2.0 and $+2.5$, i.e., at opposite edges of the one-exciton band. Note that in general as the excitation energy is tuned to higher energies, the positive part of the $\Delta A(E)$ spectrum (which is dominated by ESA) shifts toward lower energies. This is qualitatively what has been observed experimentally.[24,25] Yet, taken as a whole, the spectra of the ideal ring and single disordered rings have not much similarity to the experimental spectra. As in a macroscopic sample one is dealing with the optical response of a huge variety of disordered aggregates, a reasonable assumption would be that one has to average over a large number of disordered B850 rings. This will be addressed below.

Ensemble of 5000 B850 Rings with Diagonal Disorder. The linear absorption spectrum and its individual contributors (see, eq 5) of an ensemble of 5000 different disordered rings with $\sigma = 0.6$ are shown in Figure 3. Now indeed the shape of the simulated spectrum is rather similar to the experimental spectrum,[24,25] which is characterized by an abruptly vanishing low-energy absorption tail and a long wing on high-energy side.

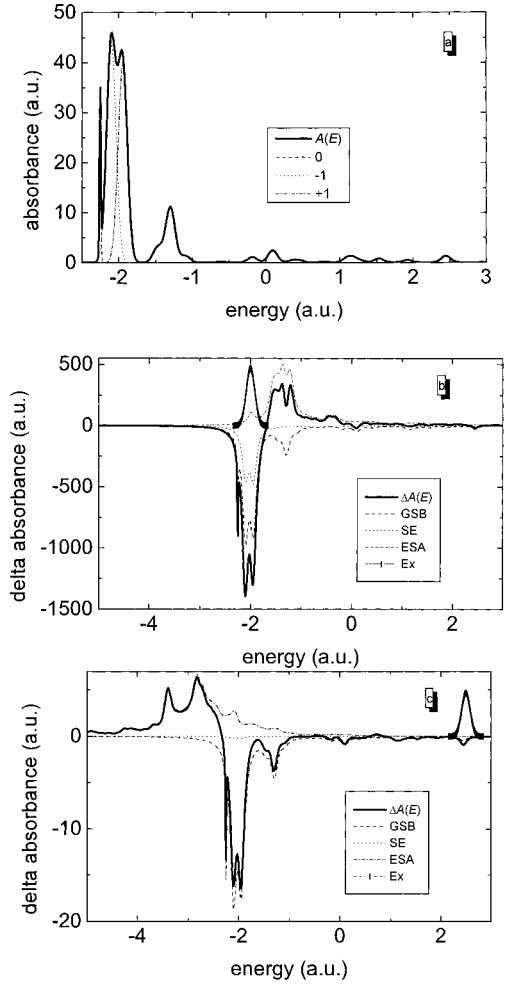

Figure 2. Simulated linear (a) and prompt nonlinear absorption difference (b and c) spectra of a single ring of 18 transition dipoles with diagonal disorder ($\sigma = 0.72$). In part a, only the contribution of $k = 0$ and $k = \pm 1$ component spectra are indicated. The position of a Gaussian excitation pulse is denoted in parts b and c with Ex ($\Gamma_{ex} = 0.2$). See text for further details.

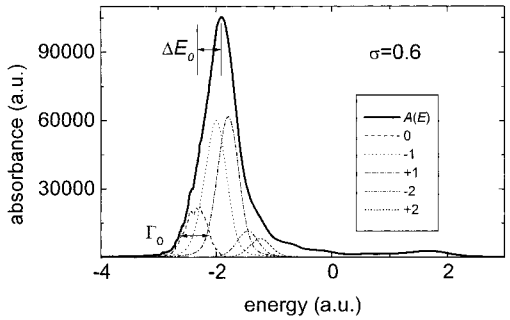

Figure 3. Simulated linear absorption spectrum of an ensemble of 5000 disordered B850 rings with standard deviation $\sigma = 0.6$. The individual transitions have homogeneous Lorentzian line shapes of the following fwhm: $\gamma_0 = 0.01$ and $\gamma = 0.12$. Indicated are the five strongest subbands contributing into the overall spectrum. The fwhm of the inhomogeneously broadened $k = 0$ subband is denoted by Γ_0 and the shift of this band relative to the overall exciton band maximum by ΔE.

Although the shape of the overall spectrum is smooth, the disorder-broadened subbands belonging to the different k transitions are well separated. The low-energy $k = \pm 1$ transitions still determine the position of the maximum of the overall spectrum. Of special interest to us here are the low-energy $k = 0$ transitions, which in accordance with ref 25, contribute only

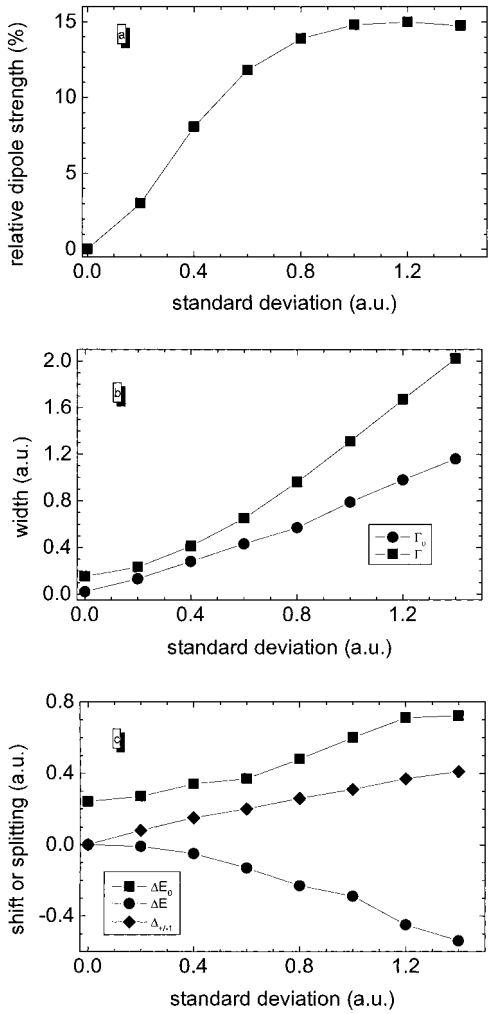

Figure 4. Relative dipole strength of the $k = 0$ subband (a), bandwidths Γ_0 and Γ (b) and different shifts ($\Delta E_0 = E_{B850} - E_0$; $\Delta E = E_{B850}(0) - E_{B850}(\sigma)$) and the splitting between the $k = \pm 1$ subbands $\Delta_{\pm 1}$ (c) calculated from the simulated linear absorption spectrum of the B850 aggregate as a function of standard deviation of diagonal disorder. Solid lines are only for the aid of the eye. See text for further details.

to the low-energy slope of the overall absorption spectrum. Steady-state narrow spectral holes can be burned into the inhomogeneously broadened B850 band exclusively in the region of these transitions.[26]

Figure 4 considers the dependence of some of the characteristics of the inhomogeneous linear absorption bands on the disorder standard deviation, σ. For the $k = 0$ subband, those characteristics are as follows: the relative dipole strength, $\mu_0^2/\sum\mu_k^2$, calculated as the integral over the $k = 0$ subband divided by the integral over the whole one-exciton absorption band (Figure 4a); the fwhm of the inhomogeneously broadened $k = 0$ subband, Γ_0 (Figure 4b); the energy gap between the overall band maximum and the peak of the $k = 0$ subband, $\Delta E_0 = E_{B850} - E_0$ (Figure 4c). The last two characteristics are defined in Figure 3. The significance of these dependencies is that they allow an estimate of the magnitude of the disorder in the B850 aggregate from independent experiments, such as hole burning[26,27] and spontaneous fluorescence quantum yield[28] studies (see below). Also plotted in Figure 4 are the overall exciton absorption fwhm, Γ (Figure 4b), the shift of the overall band maximum, ΔE, and the splitting of the $k = \pm 1$ subbands, $\Delta_{\pm 1}$ (Figure 4c) as a function of disorder.

The relative dipole strength of the $k = 0$ subband increases initially almost proportionally to the disorder until at around σ

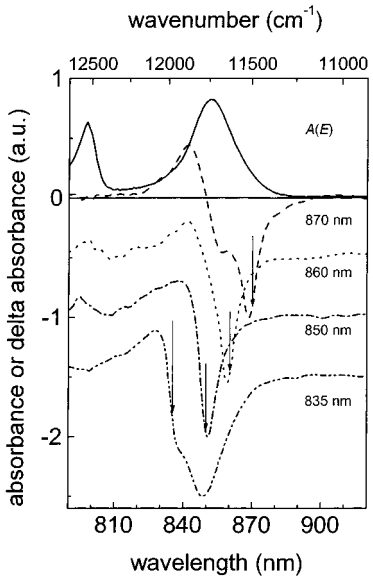

Figure 5. Experimental early-time absorption difference spectra at 8 K as a function of excitation wavelength. The spectra are recorded at 50−100 fs before the excitation pulse reaches its maximum. Spectral bandwidth of the pump pulse is 5 nm. For clarity, the delta absorbance spectra at different excitation wavelengths (denoted by arrows) are normalized and shifted vertically relative to each other. The linear absorption spectrum $A(E)$ of LH2 chromatophores at 8 K[25] is plotted for reference.

$= 0.8-1.0$ it saturates at a level of about 15%. The apparent decrease of the dipole strength at the largest disorder is due to disorder-induced localization of the exciton. With disorder, the absorption bands broaden and shift nonlinearly toward lower energies. At $\sigma = 0.7$, the overall width of the absorption spectrum is a factor of 2 times less and the width of the $k = 0$ subband is a factor of 3.3 times less than the width of the distribution function of the offset energies, Γ_{in}. The fwhm of the distribution function is defined as $\Gamma_{in} = 2\sqrt{2\ln 2}\sigma$. This is the famous exchange narrowing phenomenon.[10] In agreement with the theory,[16,17] the splitting of the $k = \pm 1$ subbands increases almost linearly over the whole considered disorder range. Note that the specific number depend on the model parameters applied.

4. Comparison with the Experiment

Selected Experimental Data. Let us first recount some of the key features of the femtosecond time-resolved experiment performed previously using spectrally selective excitation,[24,25,28] which demonstrate the disordered nature of the B850 antenna system. At low temperatures, the shapes of the initial (zero time) $\Delta A(E)$ spectra vary considerably as a function of the excitation wavelength within the Q_y linear absorption band of B850 (Figure 5). When the excitation is close to the red edge of the linear absorption spectrum, the bleached GSB/SE part of the absorption difference spectrum reveals a characteristic shape with a shoulder that is at higher energy, but that is not coincident with the peak in the linear absorption spectrum. The bleaching band narrows gradually and shifts to the blue along with the pump wavelength. The narrowest bleaching bands are observed at excitation wavelengths between 845 and 855 nm, just around the maximum of the linear absorption spectrum at about $\lambda_{abs} =$ 852 nm. The GSB/SE band broadens again and eventually splits into two bands when the pump wavelength is less than about 840 nm. The ESA intensity enhances gradually relative to the GSB/SE signal with increasing the excitation wavelength. It is also instructive to notice the following. (i) The shape of the bleaching spectrum is different when one compares the spectra excited at equal energies above and below λ_{abs}. Using excitation on the blue side of the peak, the initial bleaching band appears almost resonant with λ_{abs}, while the isosbestic point (the point where the absorption difference spectrum changes its sign) is close to the excitation wavelength, λ_{ex}. In contrast, the red edge excitation results in isosbestic point being very near to the λ_{abs}. (ii) If $\lambda_{ex} > \lambda_{abs}$, the bleaching appears mostly at the high-energy side of the excitation, and visa versa, bleaching is largely toward lower energies, if $\lambda_{ex} < \lambda_{abs}$. A number of these experimental findings can be reproduced by simulated $\Delta A(E)$ spectra, using $0.4 \leq \sigma \leq 0.8$ (not shown). However, there is a notable disagreement in the failure of the model to repeat the features outlined in (i) and (ii) above. This points out that further evaluation of the model is needed.

The necessity of the model improvements is further reinforced by large variations of the estimates of the diagonal disorder from different spectroscopy data interpreted via the present model. In ref 25, it was concluded that the shape of the linear absorption spectrum of B850 at 8 K could be well reproduced by taking $\sigma \approx 0.7$. This speculation is qualitatively consistent with the fluorescence quantum yield data[29] showing that in *Rb. sphaeroides* at 4 K, the dipole strength of the emitting state of LH2 corresponds to a total of 2−3 BChl monomers. If this is true then $\sigma \geq 0.55$, according to Figure 4a. However, the hole-burning results at 4 K[25] imply that the relative intensity of the $k = 0$ subband is only 3%. This corresponds to a much smaller disorder of $\sigma \approx 0.2$. Moreover, different hole-burning results seem to disagree with each other. So, the $k = 0$ subband shift and width, $\Delta E_0 = 185 \pm 10$ cm^{-1} and $\Gamma_0 = 135 \pm 10$ cm^{-1}, respectively, estimated from the hole burning measurements[25] support a much larger disorder than $\sigma = 0.2$, unless the nearest-neighbor coupling energy is taken to be unreasonably large. For example, in order to fit the above data with our model assuming $\sigma = 0.2$, a nearest-neighbor coupling energy of about 685 cm^{-1} (from the band shift data) or 1230 cm^{-1} (from the bandwidth data) must be applied. We further show that this inconsistency can be partly resolved by assuming a simultaneous presence in the system of an additional energetic disorder.

Two Types of Disorder. So far, we have considered a random distribution of site energies within the B850 ring aggregate. The distribution of site energies is unique for each ring in a large ensemble, but they all have the same mean energy equal to $E + D$ (see eq 2). (In the described model calculations this mean energy has been arbitrarily set equal to zero.) We now generalize our model assuming that also the solvent shift D may have a random supplement. This assumption is rather natural taking into account that in photosynthetic membranes different antenna proteins may experience slightly different surroundings which drive their spectroscopic properties. According to this hypothesis, eq 2 can be modified as

$$H_{ii} = E + D + \delta_i^e + \delta_e \tag{8}$$

Equation 8 assumes that the solvent shift offset energy δ_e is common for all chromophores of a given B850 aggregate, just shifting the spectrum of the aggregate as a whole. In contrast, δ_i^e differs for various chromophores of the given aggregate. The aspects of configuration averaging are emphasized by using the superscript e in δ_i^e. In what follows, the corresponding disorder distributions, $P(\delta_e)$ and $P(\delta_i^e)$, shall be named as external and internal disorder, respectively. If, like δ_i^e, the random solvent shifts follow a Gaussian distribution, the

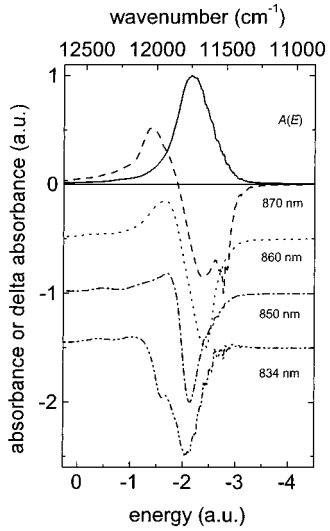

Figure 6. Simulated linear absorption and nonlinear absorption difference spectra of disordered B850 aggregates as a function of excitation vawelength. The spectra presented are averaged over 1800 aggregates. The model parameters used are as follows: $\sigma_i = 0.56$, $\sigma_e = 0.14$, $\gamma_0 = 0.02$, $\gamma = 0.15$, $\Gamma_{ex} = 0.2$.

distribution $P(\delta_e)$ can be characterized with a standard deviation, σ_e. With the above physically sound modification of the model, most of the seemingly anomalous experimental data can be rationalized as described below.

Simulation of the Prompt $\Delta A(E)$ Spectra of B850 as a Function of Excitation Energy. It is important to realize that from the parameters of Figure 4, the relative intensity of the $k = 0$ subband and its shift from the overall band maximum are only sensitive to internal disorder, whereas the bandwidth depends on both internal and external disorder. This statement is true when there is a strong coupling between the molecules in a given B850 ring and a very weak coupling between the molecules in different rings. In this case, it also turns out that the $\Delta A(E)$ spectrum is rather sensitive to the ratio of internal and external disorders.

Combining the fluorescence quantum yield[29] and the hole-burning $k = 0$ band shift data[26] with the results of our model calculations, the standard deviation characterizing internal disorder in the B850 ring can be chosen equal to $\sigma_i = 0.55 \pm 0.05$. For an educated guess of σ_e, one may try to use a well-known relation connecting the bandwidths of the Gaussian contributors into the total bandwidth, $\Gamma_0^2 = \Gamma_i^2 + \Gamma_e^2$. Given that Γ_0 is the best-fitted $k = 0$ bandwidth, when only internal disorder has been taken into account, as in ref 25, one obtains $\sigma_e \approx 0.15$. It should be mentioned, however, that this procedure is not generally correct, because the internal disorder is affected by exchange narrowing, while the external disorder is not. The criterion of acceptability is $\Gamma_i/V \gg 1$, which is only vaguely fulfilled in the present case with $\Gamma_i/V \approx 1.7$. This implies that while the assumption may be qualitatively useful, it is unlikely to be quantitatively accurate.

In Figure 6, the simulated $\Delta A(E)$ spectra are demonstrated at different excitation wavelengths applying $\sigma_i = 0.56$ and $\sigma_e = 0.14$. The same interaction matrix as in ref 21 was used, except that the intradimer and interdimer coupling energies were adjusted closer to each other, in accordance with more recent corrections.[5,30] The estimates of the homogeneous line widths were obtained from the femtosecond absorption difference[24,25] and hole-burning[26] experiments.

Evident is a good qualitative agreement between the experimental and calculated spectra when comparing Figures 5 and 6. There are also clear quantitative differences, which can be further resolved by taking into account some of the factors that affect the real life experiment and are missing from the present model. For example, due to the ultrafast exciton population relaxation, which occurs already during the femtosecond excitation pulse,[24,25] the actual populations of the exciton levels in the experimental spectra differ from those assumed in the simulation. Another aspect is the obvious need to use more realistic homogeneous line shapes that explicitly include exciton−phonon coupling effects (see below). Finally, there are sample to sample variations of the experimental spectra measured under presumably identical conditions,[24,25,28] mainly affecting the ESA region.

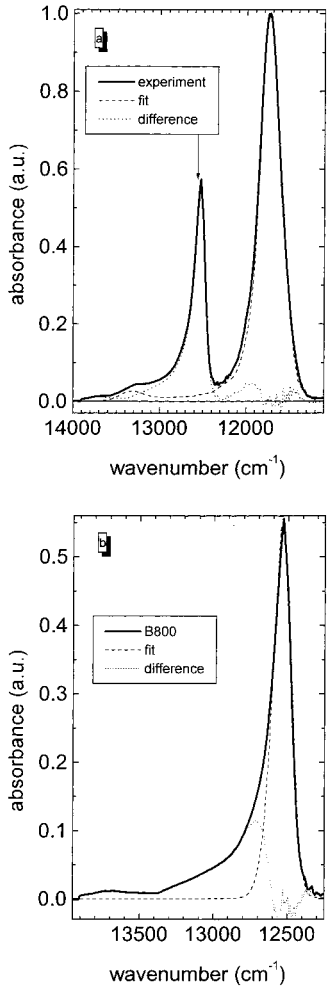

Figure 7. (a) Experimental linear absorption spectrum of LH2 chromatophores at 8 K[25] (solid line) together with the best-fitted simulated absorption spectrum of B850 excitons (dashed line) and their difference (dotted line). Arrow indicates estimated Q_y transition energy of uncoupled BChl molecules in the LH2 protein surroundings. (b) Fitting of the B800 absorption band (obtained from Figure 7a after the contribution of the B850 exciton band is subtracted from the experimental spectrum, solid line) with the simulated spectrum (dashed line). The difference of the simulated and observed spectra are shown as a dotted line. The simulated spectra presented are averaged over 5000 aggregates.

Linear Absorption Spectrum of B850. Figure 7a shows the experimental ground-state absorption spectrum of LH2-only chromatophores recorded at 8 K and presented on a frequency scale along with the calculated absorption spectrum of an ensemble of disordered B850 aggregates using the same parameters as in the previous section. The intensity scale of the simulated spectrum has been multiplied with a factor

proportional to the frequency in order to obtain a correct comparison with the measured spectrum. The fitting of the simulated spectrum to the experimental one was performed in two steps. First, the B850 absorption peaks were aligned together. Then the shapes of the spectra were matched by stretching or compressing of one spectral axis relative to the other. The difference between the measured and simulated spectra is also plotted in Figure 7a.

As seen, the experimental and calculated spectra fit each other rather well around the B850 absorption band. There also seems to be a match between the B850 one-exciton band edge and the hump in the measured spectrum around 750−755 nm. To our knowledge, the origin of this band has never been elaborated. Usually, it is assigned to a vibrational sideband or a small fraction of nonfunctional BChl molecules in the sample. Assuming that the present fitting is correct, the discussed band is mostly due to the high-energy boundary of the B850 one-exciton manifold. At intermediate wavelengths the strong B800 absorption band dominates.

As with the nonlinear spectra, the fitting of the linear absorption spectrum may be further improved by using more realistic homogeneous line shapes and by careful balancing the extent of internal and external disorders. It is, however, immaterial to pursue these improvements here, because the basic conclusions remain the same. The present fitting returns $V = 375 \pm 25$ cm^{-1}, as for the coupling energy between the nearest-neighbor BChl molecules and $E_0 = 12\,565$ cm^{-1} (corresponding to 795.9 nm in the wavelength scale), as for the Q_y transition energy of an isolated (uncoupled to other BChls) BChl molecule in the protein surroundings. The latter energy is indicated in Figure 7a by arrow. A simplifying assumption has been made that the transition energies of all uncoupled BChl molecules in the aggregate are the same. With the obtained parameters, we get $\mu_0^2/\sum\mu_k^2 \approx 10.4\%$, $\Delta E_0 \approx 173$ cm^{-1}, $\Delta_{\pm 1} \approx 89$ cm^{-1}, and $\Gamma_0 \approx 181$ cm^{-1}. The first three parameters are in reasonable agreement with the fluorescence quantum yield,[29] hole burning,[26] and single molecule spectroscopy[3] data, respectively. There is, however, a discrepancy between the calculated and estimated from the hole-burning measurements Γ_0 values, which we cannot explain within the present model.

Evaluation of the B800 Linear Absorption Spectrum. The fitting procedure described above (Figure 7a) allows also the shape of the linear absorption spectrum of excitons in the 9-chromophore B800 ring aggregate to be determined. The spectrum in Figure 7b is obtained by subtracting the calculated B850 absorption spectrum in Figure 7a from the normalized experimental absorption spectrum of LH2 complexes. As was already mentioned, this procedure implicitly assumes a very weak perturbation of the B850 excitons by the B800 excitons and visa versa.

The shape of the B800 absorption band is radically different from the shape of the B850 absorption band discussed before. It has a peculiar asymmetric shape with a long tail on the high-energy side. The disordered exciton model calculations, using the hole burning data[27] as a reference, imply that these major spectral shape differences are not a result of variant σ_i/V or σ_e/V ratios in the B850 and B800 aggregates. As demonstrated in Figure 7b, with the present model, we are able to reproduce only the low-energy side of the B800 band reasonably well. The model totally fails to reconstruct the asymmetric high-energy tail of the spectrum. The difference spectrum (the B800 absorption band minus the best simulated spectrum) exposes the shape of the sideband, which peaks at about 12 710 cm^{-1}. An analysis given in the next section allows us to suggest that this sideband and, thus, the asymmetry of the B800 absorption band, have primarily a vibrational origin. This is why the shape of the B800 band cannot be reproduced by the present model, which completely ignores exciton−vibrational interactions.

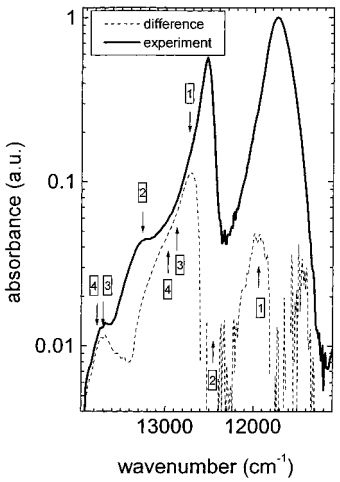

Figure 8. Experimental linear absorption spectrum of LH2 chromatophores measured at 8 K[25] (solid line) together with the difference spectrum (dashed line) resulting from subtraction of the best-fitted simulated absorption spectrum (data taken from Figures 7a,b). Indicated are possible positions of four vibronic transitions. The simulated spectra presented are averaged over 5000 aggregates. Note the logarithmic intensity scale. See text for details.

Coupling of LH2 Excitons with High-Energy Intramolecular Vibrations of Bacteriochlorophyll *a*. Figure 8 generalizes the data of Figure 7, a and b. Absorbance is given in the logarithmic scale in order to amplify the weak tails of the experimental absorption spectrum of LH2 complexes and substructures of the difference spectrum. The latter is obtained after subtraction of the best-fitted simulated spectrum from the experimental spectrum; i.e., it represents the parts of the measured spectrum that have not been described by the present model. Also shown in Figure 8 are two series of BChl intramolecular vibrational frequencies, which are designated either by upward arrows (B850 absorption band peaks) or by downward arrows (B800 absorption band peaks). The four vibrations indicated are the ones most strongly coupled with the BChl Q_y electronic transition in frozen solutions:[31] 180, 750, 1150, and 1250 cm^{-1} (numbered by 1, 2, 3, and 4, respectively).

It can be seen that there is a sensible correlation between the peaks in the difference spectra and the positions of the arrows in Figure 8. The intensities of the peaks in the difference spectrum relative to each other and to the intensity of the B850 and B800 peaks should not be taken too seriously due to the simulation uncertainties and limited signal-to-noise ratio. These intensities are, nevertheless, reasonable and they positively correlate with other known data.[26,31]

From Figure 8, it also becomes clear that the weak sideband of the B800 band at about 13 700 cm^{-1} or 729.9 nm is most probably caused by the 1150 and 1250 cm^{-1} intramolecular vibrations combined, which are coupled to the excitons in the B800 ring. The high-energy edge of the B850 exciton band and the 750 cm^{-1} vibration, which builds on the B800 excitons, contribute into the sideband around 750−755 nm. Figure 8 also provides a simple explanation for the strong asymmetry of the B800 absorption band shape. In the 12 700−13 100 cm^{-1} spectral region, several vibrations overlap, which are coupled to excitons in different rings. So, the actual asymmetry of the absorption spectrum of B800 excitons due to exciton−vibrational coupling may be less than seen in the spectrum. Part

of its apparent asymmetry is probably caused by the vibrations interacting with the B850 excitons.

5. Discussion

It is instructive to briefly consider some of the values of the model parameters obtained from the fitting of the simulated linear and nonlinear absorption spectra to the experimental data. The most important parameters determined are $V^{850} = 375$ cm^{-1}, $V^{800} = -23$ cm^{-1}; $E_0^{850} = 12\,565$ cm^{-1}, $E_0^{800} = 12\,580$ cm^{-1}; $\sigma_i^{850} \approx 216$ cm^{-1}, $\sigma_i^{800} \approx 46$ cm^{-1}; $\sigma_e^{850} \approx 54$ cm^{-1}, $\sigma_e^{800} \approx 46$ cm^{-1}. The superscript denotes which of the parameters belongs to the B850 or B800 aggregate. By conveying the standard deviation into equivalent fwhm, one gets: $\Gamma_i^{850} \approx 507$ cm^{-1}, $\Gamma_i^{800} \approx 108$ cm^{-1}, $\Gamma_e^{850} \approx 127$ cm^{-1}, $\Gamma_e^{800} \approx 108$ cm^{-1}.

The coupling constant V^{850} acquired from the fitting is almost 20−30% larger than the one calculated in the dipole−dipole interaction approximation.[5,21,23] At the same time, V^{800} obtained from the fitting turns out to be practically the same as calculated in the point−dipole approximation. This correlates well with a much tighter structure of the B850 aggregate when compared with the B800 aggregate.[4] In the latter case, the point−dipole approximation is a perfect tool, while in the case of B850 a contribution of exchange interactions cannot be overlooked.[30]

We notice that the standard deviation of the external disorder, σ_e, is rather similar for the B850 and B800 aggregates. This is not surprising, as both aggregates are embedded into the same protein subcomplex. A comparison of the internal disorder parameter reveals that the deviations of the local surroundings of BChl molecules in the B850 and B800 aggregates can be much more prominent. Also, the ratio, V/σ_i, that determines the average size of the exciton varies significantly, being almost 4 times larger in the B850 ring than in the B800 ring: $(V/\sigma_i)^{B850} \approx 1.8$ and $(V/\sigma_i)^{B800} \approx 0.5$, respectively. These numbers correlate favorably with other data. Notably, using hole burning[26,27] and single molecule spectroscopy[3] techniques, it has been demonstrated that at low temperatures excitons in B850 are well spread over the whole aggregate, while excited states of the B800 ring of pigments are mainly localized on individual BChl molecules.

Given the Q_y transition energy of BChl molecules in a vacuum[32] of about 13 340 cm^{-1}, the calculated site-energy values, and the B850 and B800 absorption peak positions, one can now more constructively approach the following long-term problem of the optical spectroscopy of light-harvesting antennas. What is the origin of a strong red shift of Q_y absorption bands of aggregated BChls in antenna proteins? From the above data, we can estimate that in B850 the contributions of the solvent (or the protein environment-induced) and interchromophore exciton coupling into the overall red shift are fairly similar: −776 cm^{-1}, as due to the solvent shift and −828 cm^{-1}, as due to the exciton coupling. In the B800 aggregate the same contributions have qualitatively different values: −761 and −49 cm^{-1}, respectively.

The remaining parameters in our numerical model are the two homogeneous exciton level widths, γ and γ_0. These parameters have been introduced into the model using estimates from previous experimental (femtosecond kinetic[4,21,24,25,29] and hole burning) data.[26,27] Using the above coupling constants, we calculate: $\gamma^{B850} \approx 58$ cm^{-1} (which corresponds to a population decay time constant of about 90 fs), $\gamma^{B800} \approx 6.9$ cm^{-1} (770 fs); $\gamma_0^{B850} \approx 1-5$ cm^{-1} (1−5 ps), $\gamma_0^{B800} \approx 2.3$ cm^{-1} (2.3 ps). The very short lifetime of the lowest $k = 0$ exciton states in both B850 and B800 needs some explanation. In B850, it probably can be interpreted as due to efficient exciton energy transfer between different LH2 complexes in the membrane. As there is only a single γ_0 parameter in our model, this rate constant, of course, should be understood as an average rate constant. In reality, a broad distribution of γ_0^{-1} lifetimes exists. In B800, the lifetime of the $k = 0$ exciton state is limited by the B800 → B850 exciton energy transfer.[27]

All the discussed parameters depend critically on the exciton coupling strength. We admit that for determining the exciton coupling energy the applied fitting procedure is somewhat arbitrary, unless the spectral position of the upper exciton band boundary is known with certainty. Recently, the upper exciton component of the B850 aggregate has been identified at 12821 cm^{-1} (780 nm) in the circular dichroism spectrum of LH2-only mutants of *Rb. sphaeroides* at 77 K.[33] We have repeated all the calculations including this extra piece of experimental evidence. Contribution of exchange interactions into the exciton coupling energy and unequal site energies of the three BCh1s in the $\alpha\beta$ pair, as suggested in ref 30, were also taken into account. A similar quality of the fitting as demonstrated above can be achieved with this refined model (not shown). However, a much weaker exciton coupling ($V^{850} \approx 250$ cm^{-1} rather than about 385 cm^{-1}) and lower site energies in the B850 ring compared to the B800 ring (medium site energy, $E_0^{850} = 12348$ cm^{-1} or 809.8 nm) should be assumed. This also results in the modification of the disorder parameters: $\sigma_i^{850} \approx 188$ cm^{-1} and $\sigma_e^{850} \approx 63$ cm^{-1}. The rest of the parameters suffer lesser modifications. In this case, the B850 excitons may contribute into the asymmetry of the B800 band, but not into the sideband around 750−755 nm.

6. Summary

The objective of this work was two-fold. First, the effects of static diagonal (energetic) disorder on linear and nonlinear optical spectra of Frenkel excitons in circular aggregates were studied by computer modeling. Second, it was demonstrated that this simplified model could successfully be used in analyzing both the ground-state absorption and the initial pump−probe absorption difference spectra of LH2 antenna proteins measured upon selective population of excitons. The simultaneous modeling of linear and nonlinear absorption spectra allows a more realistic evaluation of the parameters governing the optical properties of antenna excitations than independent fitting of the individual spectra. The present work reinforces the importance of static diagonal disorder in describing the spectral properties of excitons in the LH2 antenna complex at low temperatures. It is somewhat surprising that two rather than a single type of disorder govern the antenna spectra. Fortunately, simultaneous fitting of the linear absorption and absorption difference spectra effectively controls both the disorder parameters. The nuclear dynamics that leads to relaxation and additional localization of excitons within the LH2 complex has not been included into the model thus far. The localization of excitons by phonons and intramolecular vibrations becomes crucial only if the spectral width of the homogeneous absorption spectrum is comparable to the exciton coupling energy.[34] This is evidently not the case in B850 aggregates at low temperature in view of large exciton coupling strength, limited vibrational structure of the spectrum, and narrow holes burned into the B850 absorption profile.[26] Also, in the B800 aggregate the main cause of exciton localization is diagonal disorder rather than coupling with lattice vibrations. We conclude that the low-temperature spectral properties of LH2 antenna aggregates are primarily determined by the details of interchromophore couplings and by the random distribution of electronic transition energies of

the chromophores. The nuclear dynamics plays only a minor role, so that in most cases, it can be considered as a weak perturbation to the disordered exciton problem. We finally remark that in the case of the weak exciton−phonon coupling, the same model that was exploited here can formally be generalized to describe excitons subject to linear exciton−phonon interaction in a harmonic lattice.[9]

Acknowledgment. Grant No. 96-35306-3569 from the U.S. Department of Agriculture made this work possible. A.F. and K.T. acknowledge also a partial support from the Estonian Science Foundation Grants No. 2271 and 3865. Thanks are due to T. Pullerits for kindly communicating the LH2 coordinates and interaction matrix data used in ref 21. This is publication No. 417 from the Arizona State University Center for the Study of Early Events in Photosynthesis.

References and Notes

(1) Timpmann, K.; Freiberg, A.; Godik, V. I. *Chem. Phys. Lett*. **1991**, *182*, 617.

(2) Freiberg, A.; Godik, V. I.; Timpmann, K. In *Progress in Photosynthesis Research*; Biggins, J., Ed.; Martinus Nijhoff: Dordrecht, The Netherlands, 1987; Vol. 1, p 45.

(3) Van Oijen, A. M.; Ketelaars, M.; Köhler, J.; Aartsma, T. J.; Schmidt, J. *Science* **1999**, *285*, 400.

(4) McDermott, G.; Prince, S. M.; Freer, A. A.; Hawthornthwaite-Lawless, A. M.; Papiz, M. Z.; Cogdell, R. J.; Isaacs, N. W. *Nature* **1995**, *374*, 517. Freer, A. A.; Prince, S. M.; Sauer, K.; Papiz, M. Z.; Hawthornthwaite-Lawless, A. M.; McDermott, G.; Cogdell, R. J. *Structure* **1996**, *4*, 449.

(5) Sundström, V.; Pullerits, T.; van Grondelle, R. *J. Phys. Chem. B* **1999**, *103*, 2327.

(6) Davydov, A. S. *Theory of Molecular Excitons*; Plenum Press: New York, 1971.

(7) Förster, T. In *Modern Quantum Chemistry III*; Sinanoglu, O., Ed.; Academic Press: New York, 1965; p 93.

(8) Fidder, H.; Knoester, J.; Wiersma, D. A. *J. Chem. Phys.* **1991**, *95*, 7880.

(9) Schreiber, M.; Toyozava, Y. *J. Phys. Soc. Jpn.* **1982**, *51*, 1528, 1537, 1544.

(10) Knapp, E. W. *Chem. Phys*. **1984**, *85*, 73.

(11) Juzeliunas, G. *Z. Phys. D*. **1988**, *8*, 379.

(12) Spano, F. C.; Mukamel, S. *Phys. Rev. Lett*. **1991**, *66*, 1197.

(13) Leegwater, J. A.; Mukamel, S. *Phys. Rev. A*, **1992**, *46*, 452.

(14) Knoester, J.; Spano, F. C. In *J-aggregates*; Kobayashi, T., Ed.; World Scientific: Singapore, 1997; p 111.

(15) Reddy, N. R. S.; Picorel, R.; Small, G. J. *J. Phys. Chem*. **1992**, *96*, 6458.

(16) Novoderezhkin, V. I.; Razjivin, A. P. *Photosynth. Res.* **1994**, *42*, 9. Dracheva, T. V.; Novoderezhkin, V. I.; Razjivin, A. P. *FEBS Lett*. **1996**, *387*, 81.

(17) Dracheva, T. V.; Novoderezhkin, V. I.; Razjivin, A. P. *Photosynth. Res.* **1996**, *49*, 269.

(18) Hu, X.; Ritz, T.; Damjanovic, A.; Schulten, K. *J. Phys. Chem. B* **1997**, *101*, 3854. Ritz, T.; Hu, X.; Damjanovic, A.; Schulten, K. *J. Lumin*. **1998**, *76* and *77*, 310.

(19) Meier, T.; Chernyak, V.; Mukamel, S. *J. Phys. Chem. B* **1997**, *101*, 7332. Meier, T., Zhao, Y., Chernyak, V., Mukamel, S. *J. Chem. Phys.* **1997**, *107*, 3876.

(20) Kühn, O.; Sundström, V. *J. Phys. Chem. B* **1997**, *101*, 3432, 4154.

(21) Chachisvilis, M.; Pullerits, T., Sundström, V. *J. Phys. Chem*. **1997**, *101*, 7275.

(22) Buck, D. R.; Savikhin, S.; Struve, W. S. *Biophys. J*. **1997**, *72*, 24.

(23) Sauer, K.; Cogdell, R. J.; Prince, S. M.; Freer, A.; Isaacs, N. W.; Scheer, H. *Photochem. Photobiol.* **1996**, *64*, 564.

(24) Freiberg, A.; Jackson, J. A.; Lin, S.; Woodbury, N. W. *J. Phys. Chem. A* **1998**, *102*, 4372.

(25) Freiberg, A.; Timpmann, K.; Lin, S.; Woodbury, N. W. *J. Phys. Chem. B* **1998**, *102*, 10974.

(26) Wu, H.-M.; Rätsep, M.; Jankowiak, R.; Cogdell, R. J.; Small, G. J. *J. Phys. Chem. B* **1997**, *101*, 7641. Wu, H.-M.; Rätsep, M.; Lee, I.-J.; Cogdell, R. J.; Small, G. J. *J. Phys. Chem. B* **1997**, *101*, 7654.

(27) De Caro, C.; Visschers, R. W.; van Grondelle, R.; Völker, S. *J. Phys. Chem.* **1994**, *98*, 10584.

(28) In addition to the published experimental data,[24,25] complementary new data are used in the present simulations to expand the experimental data set.

(29) Monshouwer, R.; Abrahamsson, M.; van Mourik, F.; van Grondelle, R. *J. Phys. Chem. B* **1997**, *101*, 7241.

(30) Scholes, G. D.; Gould, I. R.; Cogdell, R. J.; Fleming, G. R. *J. Phys. Chem. B* **1999**, *103*, 2543.

(31) Renge, I.; Mauring, K.; Avarmaa, R. *J. Lumin*. **1987**, *37*, 207. Avarmaa, R.; Renge, I. *Proc. Acad. Sci. Estonian SSR. Phys. Math*. **1986**, *35*, 432.

(32) Renge, I. *J. Photochem. Photobiol. A: Chem*. **1992**, *69*, 135.

(33) Koolhaas, M. H. C.; Frese, R. N.; Fowler, G. J. S.; Bibby, T. A.; Georgakopoulou, S.; van der Zwan, G., Hunter, C., N.; van Grondelle, R. *Biochemistry* **1998**, *37*, 4693.

(34) Sumi, H. *J. Phys. Soc. Jpn.* **1975**, *38*, 825.